Spectrum of Engineering Sciences
ISSN (e) 3007-3138 (p) 3007-312X Volume 4, Issue 1, 2026

STRUCTURAL AND OPTOELECTRONIC PROPERTIES OF CHALCOGENIDE PEROVSKITES; A DFT STUDY

Sheraz Mehmood[*1], Abdul Qadeer[2], Muhammad Fahad Hayat[3], Baqir Hussain[4], Muneer Ahmad[5], Aizaz Ahmad[6]

[*1]*Lecturer in Physics, Department of Physics Institute of Physics, Bahauddin Zakariya University, Multan*
[2]*Lecturer in Chemistry, Department of Chemistry Ghazi university Dera ghazi khan*
[3,4,5,6]*Department of Chemistry Ghazi University Dera Ghazi Khan*

[*1]sherazmehmood065@gmail.com, [2]abdulqadeerchandia3344@gmail.com, [3]fahadhayat201@gmail.com, [4]s9118439@gmail.com, [5]aslammuneer754@gmail.com, [6]maizazkhantalpur@gmail.com

DOI: https://doi.org/10.5281/zenodo.18358099

Keywords
DFT (Density functional theory); PBE-GGA (Perdew Burke Ernzehof- Generalized Gradient Approximation); VESTA (Visualization for Electronic and Structural Analysis); CASTEP (Cambridge Serial Total Energy Package)

Article History
Received: 29 November 2025
Accepted: 09 January 2026
Published: 24 January 2026

Copyright @Author
Corresponding Author: *
Sheraz Mehmood

Abstract

The structural, optical, electronic and mechanical properties of barium bases chalcogenide material $BaZrS_3$ have been investigated by utilizing the first principle simulation which is based on density functional theory (DFT) with framework of CASTEP code by using Perdew-Burke-Enernhoff generalized gradient approximation (PBE-GGA) functional. Lattice constant of the sample $BaZrS_3$ have been found a=b=c=5.066 A° with the bond angle $\alpha=\beta=\gamma=90°$. It has been found our material is stable in cubic phase structure with energy of -2808.93eV with the unit cell volume of 129.72 $(A°)^3$. This material have direct band gap of energy 0.458eV. In the range of energy from 0–60eV, the Kramer Kroning relation is best way to calculate parameters such as dielectric function, refractive coefficient, absorption coefficient, reflectivity, optical conductivity and energy loss function in order to know their optical performance. The calculated mechanical properties indicate that the material $BaZrS_3$ is found mechanically stable and all the elastic constants have positive values and elastic anisotropic value is 0.158. The calculated poisson ratio represents the brittle nature of material $BaZrS_3$. The B_H/G_H shows the value of 1.9 which also indicates the ductile nature of $BaZrS_3$. The stability and conductivity of this material is also confirmed by its total energy value. The partial density of states also describes that by doping the band gap energies are reduced. It can cause to increment in conductivity of compound $BaZrS_3$. By studying these characteristics, we found that our material is chemically stable and can be used in storage devices. The outcomes of results for our material $BaZrS_3$ shows that because of suitable band gap high absorption coefficient value making it a best option for renewable energy harvesting devices such as photovoltaic devices. Its composition also makes it a candidate to be used in semiconductor devices.

1.1 Introduction

Energy is important component of life and we commit with energy for daily use. Global energy consumption induction shows energy consumption 10^{13} W/ years. It is estimated that by

the year 2040 the world energy consumption will increase 40–50%. As we know that conventional energy sources are limited and if continue to use them in similar way then in future they will not be able to meet our energy needs. For conventional sources we are using fossil fuels and they are a cause of environmental pollution. They are producing the green houses gasses which are a cause of global warming and are increasing the entropy. Due to this we are facing a lot of problems like climate change, easing sea level and extreme weather. The gasses emitted from the fossil fuels are also the cause of acid rain. These factors argue us to discover alternative energy sources in order to replace the fossil fuels [1]. The step by step changing in the perovskite is described by diagram 1.1

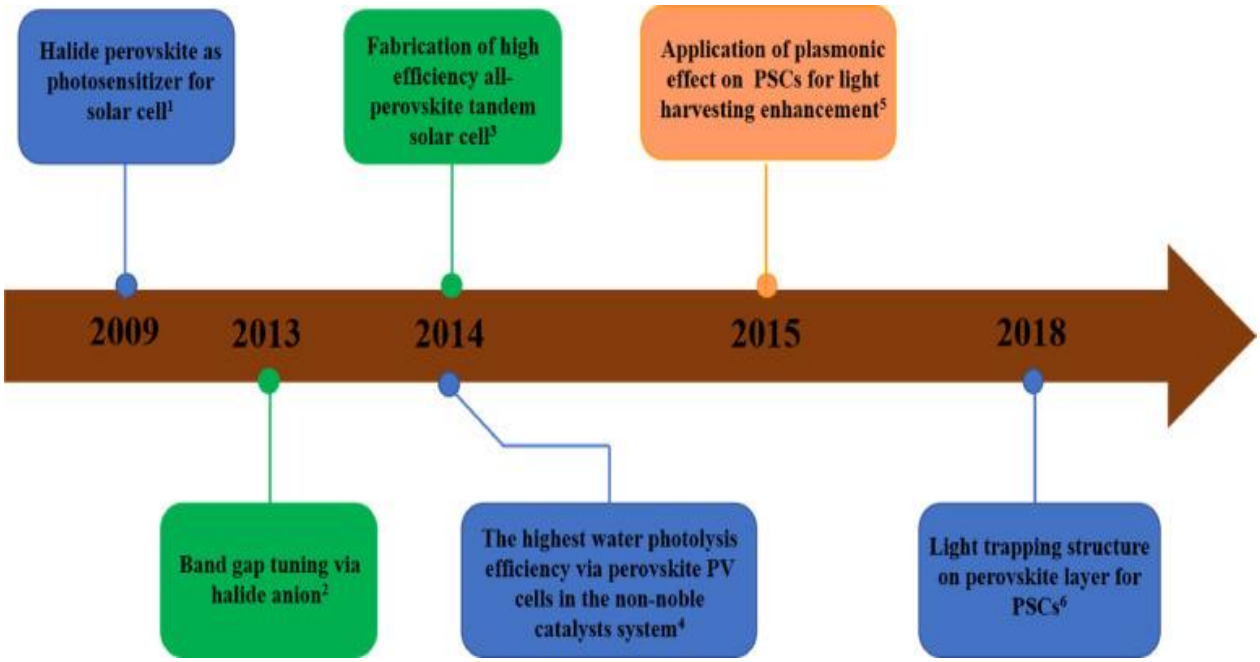

Figure 1.1History of Perovskite [1]

Due to these problematic effects, the extendable energy sources such as wind energy, sun light hydral power have attained the great attention. From all these energy sources the energy from sun is used all over the world. It is a pure source of energy. The amount of solar energy that comes from sun in one hour is more than the total consumption of planet earth is only one year. Planet earth gains solar energy 163.6W per m^2. We can illuminate the whole world by using 150W lamp on each meter square [1,2]. It implies that from whole Sahara desert if 1% area is covered with solar panels then it will be enough to provide power to world. The sun provides us heat and light energy (photons) which are enough to meet our demands for energy. So we need to change this energy obtaining from sun into other forms of energy like electricity.

The solar cell technology development could be seen when, in 1839, a French Physicist Becquerel observed the photovoltaic effect. He noticed that when the light coming from the sun drop on electrode a voltage was observed when he was noticing the properties of electrode made up of solid material in the electrolytic solution [19]. After the discovery of this effect Fritts made the first solar cell by involving the very thin coating of gold on substrate of selenium.

These energy sources can be used again and again and there is no danger for their shortage. These energy sources are very common nowadays such as solar, wind, hydro, geothermal and biomass. These

are sustainable sources and can reduce our dependency on fossil fuels. Among all these the solar energy is very commonly used nowadays. Earth attains a large amount of energy directly from the sun that is known as solar constant. It is the solar energy that falls on the unit area of earth and its value is about 1400kWm^{-2}. This energy can be used to produce electricity and can run the power plants. Photovoltaic cells respond these solar energy and electricity is produced. Some renewable energy sources are shown in figure 1.2.

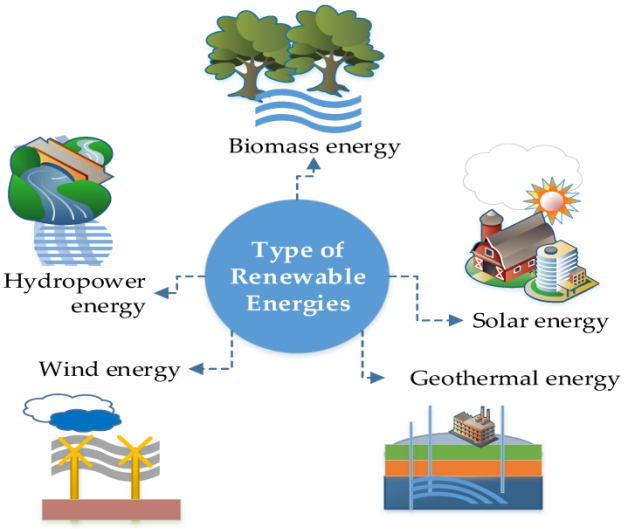

Figure 1.2 Renewable Energy Sources [1]

This work provides a comprehensive first-principles investigation of the structural, electronic, optical, and mechanical properties of the lead-free chalcogenide perovskite $BaZrS_3$ using density functional theory within the PBE-GGA framework. Unlike prior studies that focused on limited physical aspects, the present study delivers an integrated analysis combining structural stability, elastic behavior, band structure, partial density of states, and a wide range of optical response functions over an extended energy range (0–60 eV). The confirmation of a direct narrow band gap (0.458 eV), high optical absorption, and favorable dielectric and conductivity characteristics highlights the strong potential of $BaZrS_3$ for optoelectronic and photovoltaic applications. Additionally, the detailed evaluation of elastic constants, Pugh's ratio, Poisson's ratio, and anisotropy index establishes the material's mechanical stability and ductile nature, which are critical for device fabrication. These findings not only enhance the fundamental understanding of chalcogenide perovskites but also position $BaZrS_3$ as a promising, environmentally friendly alternative to conventional halide perovskites for next-generation renewable energy and semiconductor technologies.

Results and Discussion

4.1 Structural Properties

The crystal structure of chalcogenide perovskite has been modified geometrically in order to achieve maximum efficiency by implementing CASTEP code by using PBE-GGA of density functional theory (DFT). The crystal structure of BaZrS3 is cubic with space group and its number P m -3m, 221 respectively. Its point group is m-3m. In figure 4.1, the basic geometry and crystal structure of BaZrS3 is shown. This structure consists of 8 atoms of Barium. The lattice parameters of BaZrS3 unit cells are shown in Table 4.1.

In first principle study, the study of geometry optimization and structural stability is an inevitable step as an outcome of calculating parameters such as energy and volume by applying

PBE-GGA method using Density Functional Theory. The total energy for material BaZrS3 appears negative which demonstrates that our investigated chalcogenide material BaZrS3 has stable structure. The Structure obtained by using VESTA Software for BaZrS3 has been displayed in figure 4.1

Table 4.1 calculated structural parameters such as optimized lattice constant, volume of unit cell and energy at equilibrium position are mentioned as:

Crystal	Method	a=b=c (A°)	c/a=c/b	α=β=γ	V(A^{O3})	E_o (eV)
$BaZrS_3$	**PBE-GGA**	5.062	1	90°	129.72	-2808.93

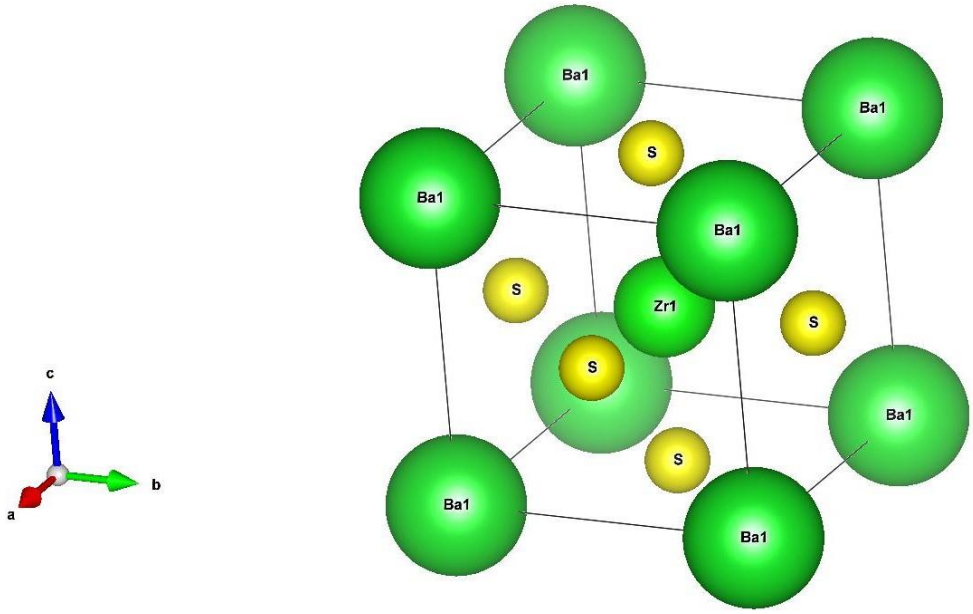

Figure 4.3Structure of BaZrS3

Table 4.1 presents the optimized structural parameters of the chalcogenide perovskite $BaZrS_3$ obtained using the PBE-GGA approach within density functional theory. The calculated lattice constants are equal along all crystallographic directions (a = b = c = 5.062 Å), confirming the cubic crystal symmetry of $BaZrS_3$. The axial ratios (c/a = c/b = 1) and interaxial angles (α = β = γ = 90°) further validate the ideal cubic perovskite structure with space group Pm–3m.

The optimized unit cell volume is found to be 129.72 $Å^3$, which is consistent with previously reported values for chalcogenide perovskites and indicates a compact and well-packed crystal structure. The equilibrium total energy of −2808.93 eV is highly negative, demonstrating the strong binding interactions among constituent atoms and confirming the thermodynamic stability of the material in its cubic phase.

Overall, these structural parameters indicate that $BaZrS_3$ forms a stable and symmetric cubic structure under equilibrium conditions. Such structural stability is a prerequisite for reliable electronic, optical, and mechanical performance, and it provides a solid foundation for the subsequent investigation of the material's optoelectronic and mechanical properties for photovoltaic and semiconductor applications.

4.2 Optical Properties

The optical properties of $BaZrS_3$ have been studied to know how a material behave when it is placed under the interaction with electromagnetic radiation in visible light range of electromagnetic

spectrum which is based on recombination rate of electron and transition rate of electron.

4.2.1 Dielectric Function

After knowing about the structural and electronic properties of $BaZrS_3$ it is now inevitable to discuss the reaction of material when the radiations interacts the particles of $BaZrS_3$ and the particles are colliding with surface of material. For example, we study the dielectric function. [86]

We study the optical characteristics of material by using dielectric function which describes the polarization and absorption characteristics of material. Mathematically it is expressed as:

$$\varepsilon(\omega) = \varepsilon_1(\omega) + i\varepsilon_2(\omega) \qquad 4.1$$

There are two parts of complex dielectric function which are real and imaginary parts. $\varepsilon_1(\omega)$ Express the real part and $\varepsilon_2(\omega)$ the imaginary part. Real part of dielectric function states that when we apply the electric field to material, a material be a polarized because of creation of dielectric poles in that material. In fact the real component describes the polarization of studying material.

Imaginary component describes the absorption of studying material $BaZrS_3$. Both component of dielectric function indicates the Kramer-Kronig relation and both are connected to each other. Both of these components such as real and imaginary component are dependent on frequency. Imaginary component is calculated by:

$$\varepsilon_2(\omega) = \frac{8}{3\pi\omega^2}\sum_{nn'}\int |P_{nn'}(\mathrm{k})|^2 \frac{dS_{\mathrm{k}}}{\Delta\omega_{nn'}(\mathrm{k})} 4.2$$

The real dielectric function for $BaZrS_3$ has been calculated by taking the values from 0 to 60eV and is expressed in figure 4.2. Real dielectric function values initially on y-axis are range from -1eV to 10eV. The value of real dielectric function dive at 3eV. We observe that spectrum of $BaZrS_3$can be described by changing height and position of peak. We also notice that after passing 3eV, the spectrum of $BaZrS_3$ demonstrate some variation and its values has been decreased and increased for little range of dielectric function and after these alternations its value become constant at 0.8eV.

The absorption rates of electromagnetic radiations on the surface of BaZrS3 have been described by virtual component of dielectric function. Initially, imaginary dielectric function has values -0.08eV and 0. After that the values increases and attains maximum value of 6.8 at 7.7eV. Before reaching to this value, its value also dip at one point and then reaches to maximum value and this point indicates highest absorption of incident light and low dispersion. Its value increases and decreases at different points and value become constant at 31.8eV. at energy axis.

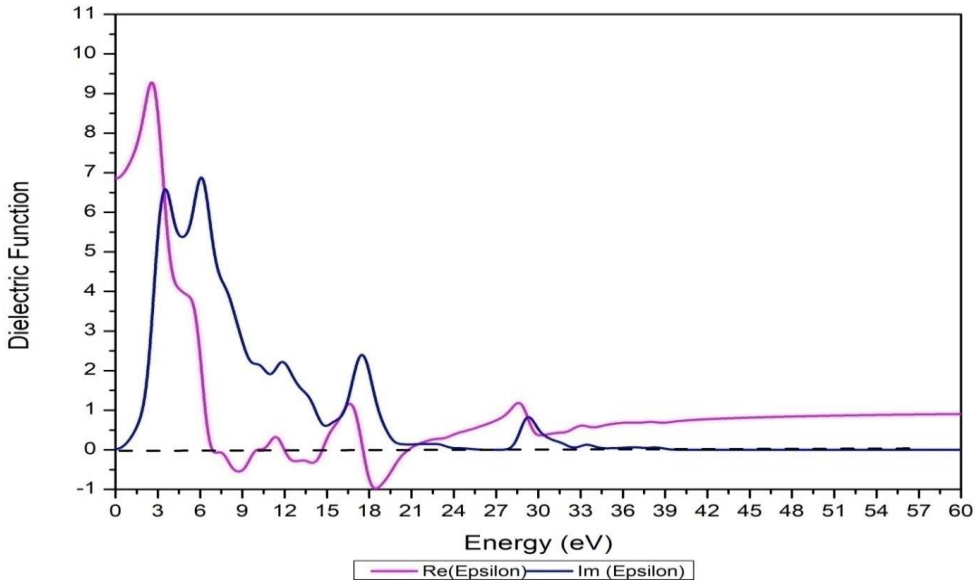

Figure 4.4Real and imaginary dielectric function of BaZrS3

4.2.2 Absorption

When the phonons are excited through the crystal then absorption of light occurs. Three optical functions such as absorption reflection and transmission originates when electromagnetic radiations (light) falls on material surface. Mathematical equation to find absorption coefficient is:

$$\alpha(\omega) = \frac{4\pi}{\lambda} k(\omega) \quad 4.3$$

We have studied the chalcogenide material $BaZrS_3$by utilizing CASTEP code along with PBE-GGA functions having range of frequencies from 0 to 60eV as shown in figure 4.3. We observe the first peak at 9.8eV for $BaZrS_3$. At different points changing has been noticed and at 20eV there is maximum peak. At 40eV the peak becomes constant.

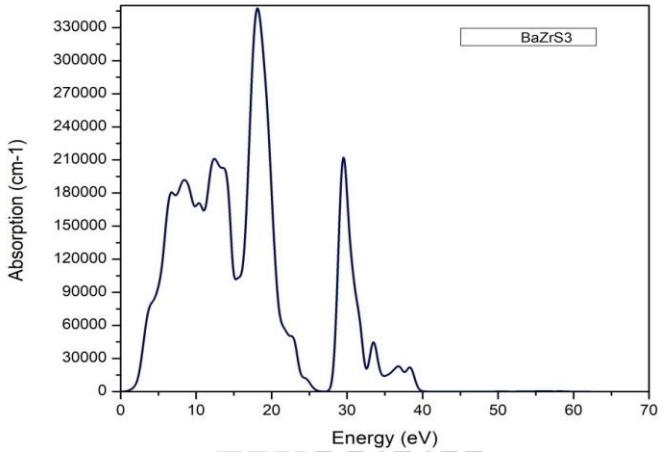

Figure 4.5Absorption coefficient for BaZrS3

4.2.3 Reflectivity

Behavior of surface of material is studied by reflectivity. We can describe how much electromagnetic radiation transmits through the material of $BaZrS_3$ and how much radiation reflects. It is found by following formula:

$$R(\omega) = \frac{|n-1|^2}{|n+1|^2} = \frac{(n-1)^2+k^2}{(n+1)^2+k^2} \quad 4.4$$

Reflectivity is expressed as ratio of incident photons energy to reflected photons energy. The reflectivity for material of $BaZrS_3$ is illustrated in figure 4.4. It is observed in different region like ultraviolet, infrared and visible region of electromagnetic spectrum. The graph shows that $BaZrS_3$has the static value of 0.2 at 0eV. We observe the different variations at different values of energy and we obtain the sharp peak of 0.63 at 21eV. In electromagnetic spectrum, these peaks are found to be in ultraviolet range.

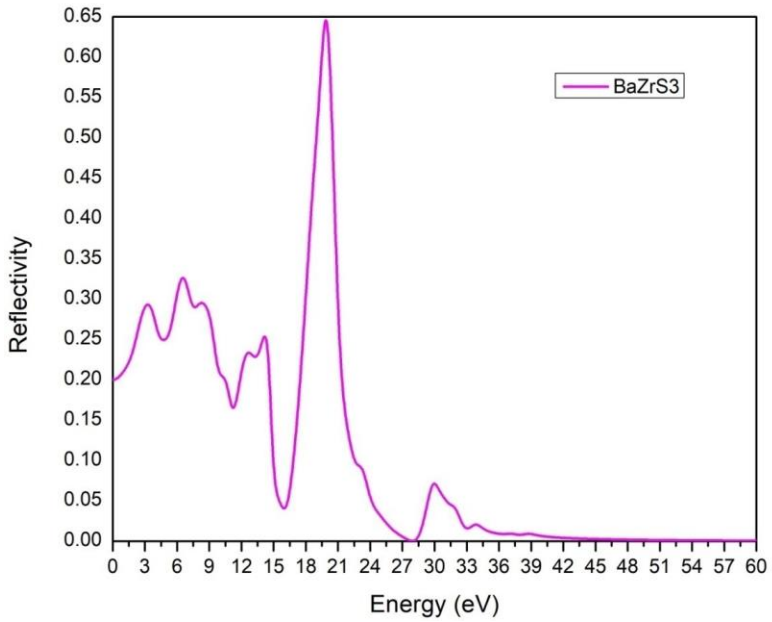

Figure 4.6Reflectivity plot for BaZrS34.2.4 Refractive Index

4.2.4 Refractive Index

The transparency of material is described by refractive index or index of refraction. The refractive index is closely related to dielectric function by following equation:

$$n(\omega) = \frac{1}{\sqrt{2}}\left[\left\{\sqrt{\varepsilon_1^2(\omega) + \varepsilon_2^2(\omega)}\right\} + \varepsilon_1(\omega)\right]^{1/2} 4.5$$

The entering of electromagnetic radiation from one material to another material at different incident and refracted angle is described by refractive index. Total internal reflection is also discussed on basis of refraction pattern. It is found that material $BaZrS_3$has value 3.13 at 3.8eV. Because of remarkable interaction among valence electrons and incident photons, $BaZrS_3$has maximum peak value also at 0eV. The value of refractive index varies at the different value of energy. The variations in value of refractive index are shown in figure 4.5.

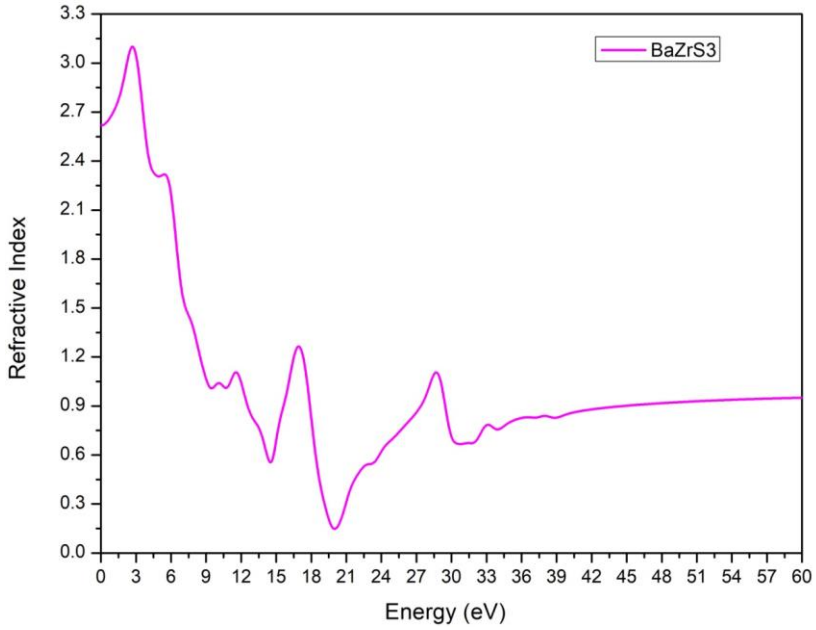

Figure 4.7Calculated Plot of refractive index for BaZrS3

4.2.5 Optical Conductivity

In order to study the behavior of electromagnetic radiation when they fall on the surface of material $BaZrS_3$and bond breakdown when the charge carriers such as electron and holes flow we use the term optical conductivity. The relation between the current density of electric field for the range of frequencies is studied by optical conductivity. The relation of optical conductivity with absorption coefficient is mathematically given as:

$$\sigma(\omega) = \frac{\alpha nc}{4\pi} \qquad 4.6$$

The optical conductivity for the material $BaZrS_3$has been displayed in figure 4.6 which represent the real value and imaginary values of optical conductivity which is related to excitation of photons when energy of these photons is increased. The optical conductivity of material $BaZrS_3$which has value is maximum 5.3$(fs)^{-1}$ AT 6.5eV and also attains this approximate value at 18.2eV. After that these values decrease and radiation falls in UV region.

The imaginary part of graph shows the optical permittivity and its ability to conduct electricity. The graph starts from zero value of conductivity at 0eV. Initially its value decreases to 2.9 (1/fs) and then increases. Its value at 19.8eV becomes maximum for this material. Its value becomes constant at 40eV. The properties have become inevitable part to develop optoelectronic devices.

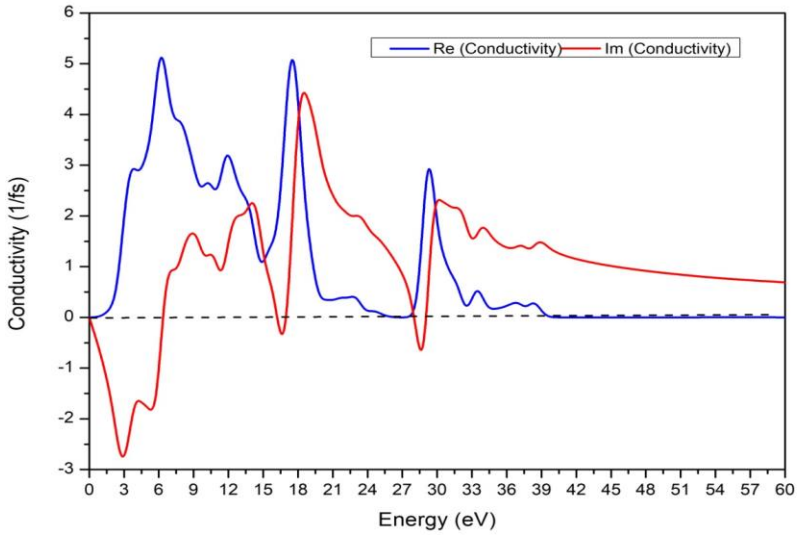

Figure 4.8Real and imaginary component of optical conductivity for BaZrS3

4.2.6 Loss Function

In order to find the additional information such as oscillation of electron in valence band and energy losses when the photons having higher frequency pass through the surface of material, we use the concept of loss function which are the optical properties of material which is related to plasma resonance frequency. When the frequency of incident light engages to plasma resonance frequency, we use the loss function. The loss function of the material is displayed in figure 4.7. In start, at zero energy the loss function has zero value. Then its value increases and becomes maximum 7.5 at 21eV then its value decreases and becomes constant at 39eV. The value of loss function is found by formula:

$$\mathrm{L}(\omega) = -Im\left(\frac{1}{\varepsilon(\omega)}\right) = \frac{\varepsilon_2(\omega)}{(\varepsilon_1(\omega))^2+(\varepsilon_2(\omega))^2} \quad 4.7$$

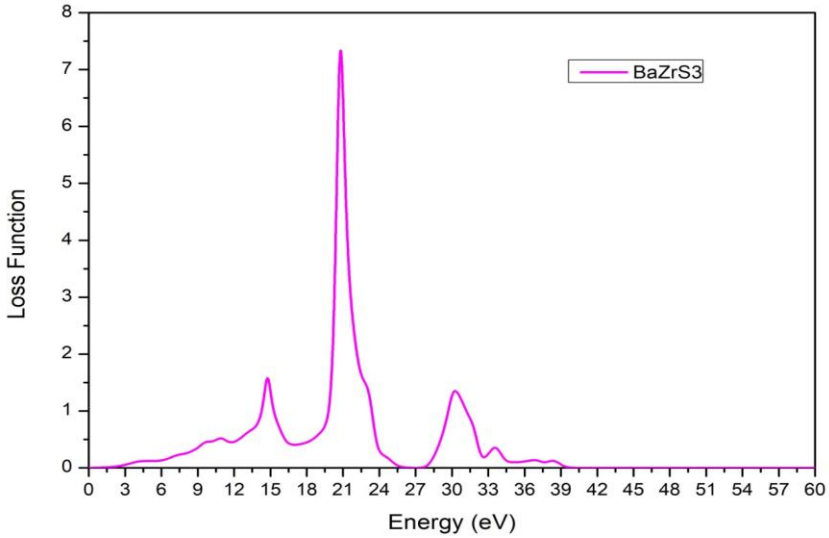

Figure 4.9Loss Function of BaZrS3

4.3 Electronic Properties

Energy band gap and band structure of chalcogenide perovskite material $BaZrS_3$have been studied with density functional theory by utilizing Perdew Burke Ernzerhof- Generalized Gradient Approximation (PBE-GGA) by CASTEP code. During the study of many semiconductor materials by using local function cause to find the inaccurate value and position of conduction band and valance band and values were different from experimental result. One of the reasons for this deviation may be columb correlation of material. For the purpose to get most accurate value of energy band structure and band structure we use the local function PBE-GGA. The studied showed that material $BaZrS_3$has direct band gap. The band gap graph is shown illustrated in figure 4.8. The electronic band structure is investigated at symmetric point in Brillouin zone. The electronic band structure (EBS) has been built with high symmetry path which is R – G – X – M – G. The band structure diagram shows that material $BaZrS_3$has direct band gap of 0. 458eV by using GGA approximation function. This band gap is found very low. The material $BaZrS_3$has been found the better solar absorber. Instead of discrete level, the solid energy levels are represented for the whole atom adjustment in the graph. It is because of motion of charge carrier between conduction and valence band. The energy gap is that area in which we cannot find any electron in bonding or anti bonding mode and it plays its role in classification of material.

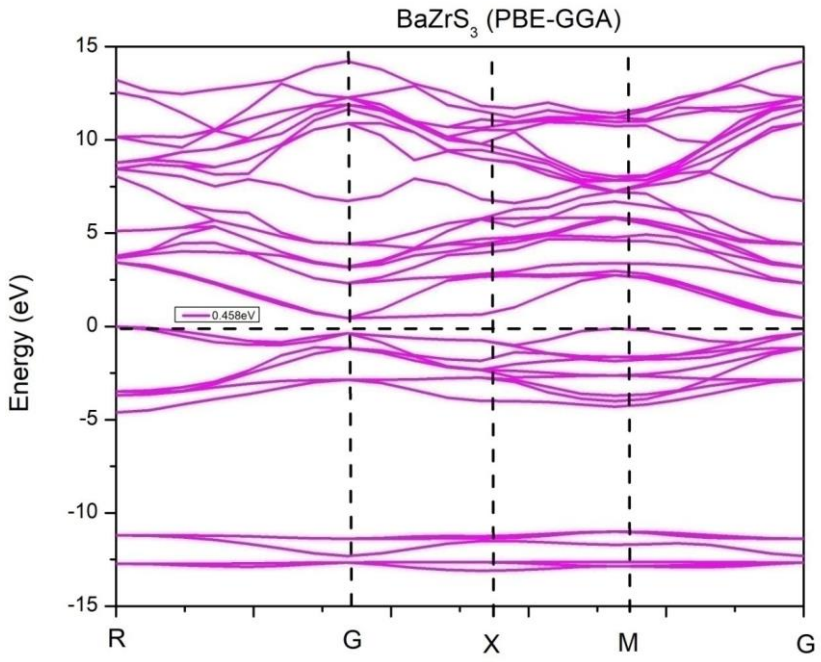

Figure 4.10 Band Structure of BaZrS3 with symmetry points

4.3.1 Partial Density of states of $BaZrS_3$

By using theoretical method generalized gradient approximation (GGA), the density of states (DOS) for $BaZrS_3$has been simulated. The electron transition between conduction band (CB) and the valence band (VB) for the material $BaZrS_3$ has been narrated by partial density of states. It also provides the information about localized state of each atom in material $BaZrS_3$.

Graph 4.3 represents the partial density of state for material $BaZrS_3$. Different states of S atom, Ba atom and Zr atoms have been taken in a range of energies -3eV to 6eV. The graph states that Ba-s atom has stronger collaboration in conduction

band because it describe the high peak in conduction region minima away from Fermi level and has smaller collaboration in valence band because of smaller peak. The d-state of Zr atom also contributes in conduction band creation as greater state has been observed in this region. The s-state of S atom take parts in formation of valence band because its more state exist in valance region at bottom of Fermi level. The S-4s is dominated in the valence band region while. The γ-point in Brilliouns zone center has the valence band and conduction band for the material $BaZrS_3$. The partial density of states (PDOS) for atoms Ba, Zr, S used in material $BaZrS_3$have been displayed in diagrams 4.9, 4.10 and 4.11.

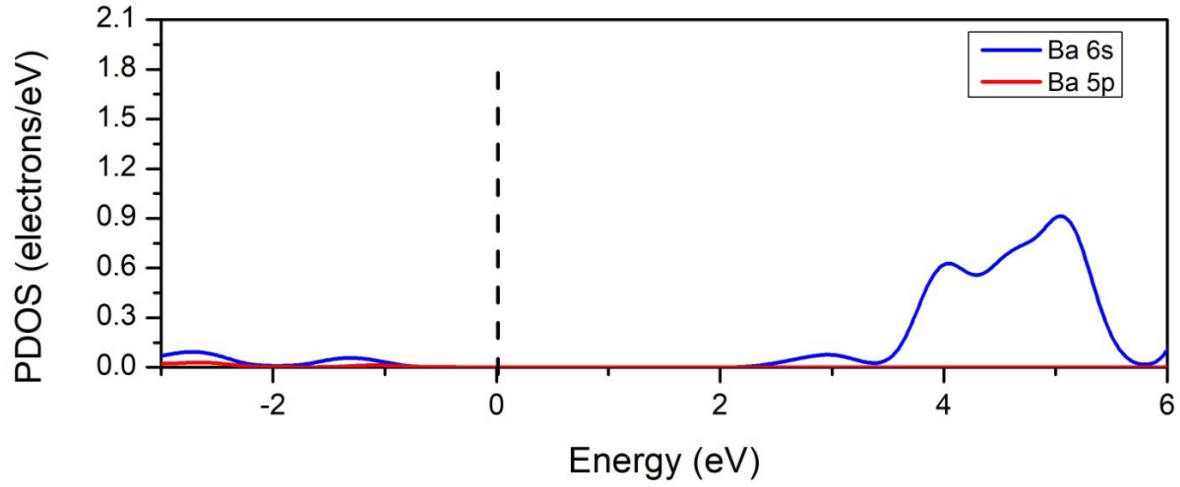

Figure 4.11 Partial density of states for Ba atom in BaZrS3

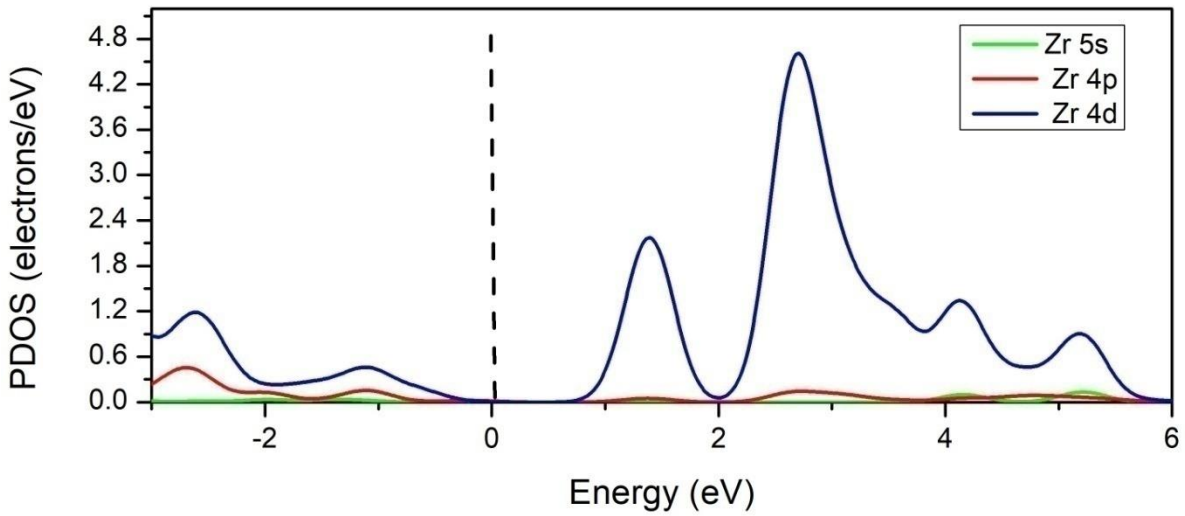

Figure 4.12Partial density of state for Zr atom in BaZrS3

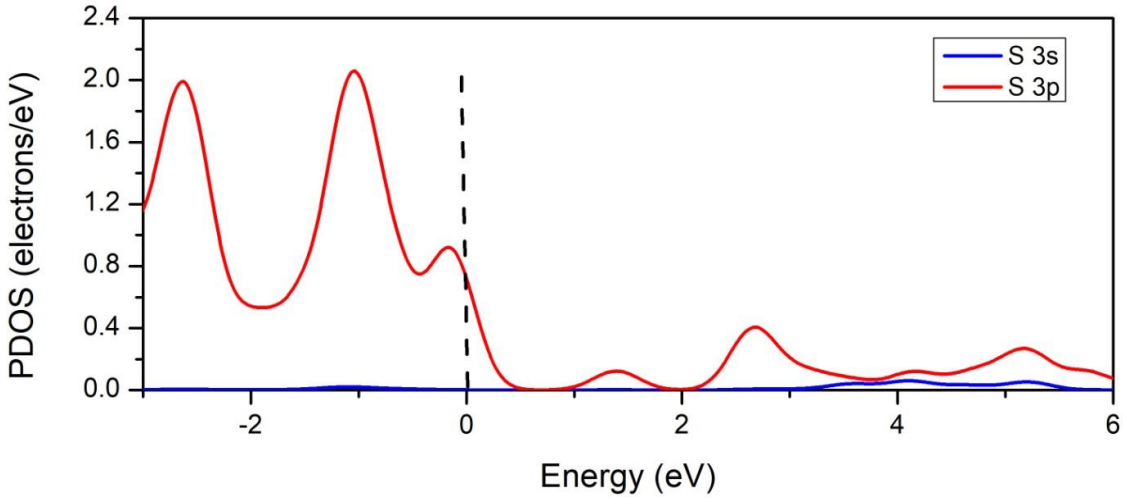

Figure 4.13Partial density of states for S atom in BaZrS3

4.4 Mechanical Properties

If we want to study the mechanical stability and dynamical properties of material then we use the parameter which is known as elastic constant which is compulsory physical parameter. It is stated as the ratio of stress to strain when we apply stress within elastic limit. Additionally, a specific bonding type present in material as well as several mechanical characteristics can also be discussed on the basis of mechanical properties and elastic constant. Different terms such as brittleness, hardness and anisotropic toughness are related to elastic constant.

Now we discuss the elastic constant C_{ij} of material $BaZrS_3$ by using CASTEP code of density functional theory simulation. The studying material $BaZrS_3$has cubic shape have elastic constant which are independent of each other are C_{11},C_{22},C_{12},C_{33},C_{44},C_{21}.

The elastic constant values for studying material $BaZrS_3$ have been mentioned in table 4.2. The table indicates that no elastic constant has negative values which mean that structure fulfill the criteria of stability. The mechanically stable structure follows the following equations:

$$C_{11}>0;C_{11}C_{22}>C_{12} \quad 4.8$$

$$C_{11}C_{22}C_{33} + 2C_{12}C_{13}C_{23} - C_{11}C^2_{23} - C_{22}C^2_{13} - C_{33}C^2_{12} > 0 \quad 4.9$$

$$C_{44}>0;\ C_{55}>0;\ C_{66}>0 \quad 4.10$$

These mentioned equations fulfill the born criteria, which show that compound $BaZrS_3$ is mechanically stable. The elastic constant of this material $BaZrS_3$can easily find out by using Bulk modulus (G) and shear modulus (B) which have anisotropic nature. These are found by implementing Voigt-Reuss-Hill process. In addition to this, the elastic modulus pairs have isotropic nature like Young's modulus; Poisson's ration can be found by utilizing bulk and shear modulus. [87]

Table 4.2 Calculated values of elastic constant in GPa for $BaZrS_3$

Compound	C_{11}	C_{12}	C_{13}	C_{21}	C_{22}	C_{23}	C_{31}	C_{32}	C_{33}	C_{44}	C_{55}	C_{66}
$BaZrS_3$	133.3	40.4	40.4	40.4	133.3	40.4	40.4	40.4	133	32.3	32.3	32.3

Table 4.2 summarizes the calculated elastic constants of the chalcogenide perovskite $BaZrS_3$, obtained using density functional theory. The elastic constants satisfy the symmetry conditions of a cubic crystal, as reflected by the equal values of $C_{11} = C_{22} = C_{33}$ (≈133 GPa), $C_{12} = C_{13} = C_{23}$ (40.4 GPa), and $C_{44} = C_{55} = C_{66}$ (32.3 GPa). This consistency confirms the reliability of the

calculations and the cubic nature of the crystal structure.

All elastic constants exhibit positive values, indicating that $BaZrS_3$ fulfills the Born mechanical stability criteria for cubic systems ($C_{11} > 0$, $C_{44} > 0$, and $C_{11} > C_{12}$). The relatively high value of C_{11} suggests strong resistance to uniaxial deformation along the principal crystallographic directions, while the moderate C_{12} value reflects the material's response to volume-conserving shear strains. The shear-related constants (C_{44}, C_{55}, and C_{66}) indicate a reasonable resistance to shape deformation, which is essential for mechanical integrity under applied stress.

Overall, the elastic constant profile demonstrates that $BaZrS_3$ is mechanically stable and elastically robust, making it a promising candidate for practical applications where structural durability and mechanical reliability are required, particularly in optoelectronic and photovoltaic devices.

The value of young modulus is used to find stiffness of material. In order to know about hardness of material we use the elastic constant C_{44}. The mechanical characteristics of solid and its hardness is defined on the basis of bulk modulus (B), young modulus (Y) and shear modulus (G). The values of E, B and G can be calculated by following equations:

$E= [9BG]/ 3[B] +[G]$ 4.11

$B= [B_V] + [B_R] /2$ 4.12

$G= [G_V + G_R] /2$ 4.13

The Poisson ratio can also be found by:

$$\text{Poisson Ratio} = \frac{[3B]- [2G]}{[6B]+ [2G]} \quad 4.14$$

Furthermore, solids and liquids have high value of bulk modulus and have same magnitude. To define the elasticity with respect to volume or object ability to undergo deformation under load, we use the bulk modulus. Bulk modulus represents the ratio of volumetric stress to strain having 3D elongation of young's modulus. The reciprocal of young's modulus 1/B defines the compressibility of material $BaZrS_3$.

In the presence of opposing forces, the ability of element to change its shape is defined by rigid modulus or shear modulus. It is the ratio of shear stress to strain. Like bulk modulus it is also used to discuss the hardness of material.

The ratio of tensile stress to strain is known as young's modulus which shows the ability of any material to deform along any one axis when opposite forces are acting on it. It is also known as elastic modulus. For the material elongation or compression we use the concept of young's modulus. The stiffness of solid material is also described by young's modulus. The values of young's (E), bulk (B) shear modulus (G), Poisson ratio compressibility coefficient are represented in table 4.3.

Table 4.3 Calculated Bulk modulus (B) and shear Modulus (G), Poisson ratio (γ), linear compressibility coefficient (β) and universal anisotropic index A^U.

System	$BaZrS_3$
B_V (GPa)	71.37
B_R (GPa)	71.37
B_H (GPa)	71.37
G_V (GPa)	37.96
G_R (GPa)	36.79
G_H (GPa)	37.37
γ	0.2741
β	0.014
A^U	0.158
B_H/ G_H	1.9

Table 4.3 presents the calculated mechanical moduli and related elastic parameters of $BaZrS_3$ obtained using the Voigt–Reuss–Hill (VRH) approximation. The bulk modulus values calculated by the Voigt (BV), Reuss (BR), and Hill (BH) schemes are identical (71.37 GPa), indicating negligible elastic anisotropy in volumetric compression and confirming the internal consistency of the calculations. This moderate bulk modulus suggests that $BaZrS_3$ possesses reasonable resistance to volume change under applied pressure.

The shear modulus values obtained from the Voigt (37.96 GPa) and Reuss (36.79 GPa) limits are very close, resulting in a Hill average shear modulus (GH) of 37.37 GPa. This reflects a stable resistance to shape deformation and further supports the mechanical robustness of the material. The calculated Poisson's ratio (γ = 0.2741) lies within the typical range for ductile materials and indicates a mixed ionic–covalent bonding nature in $BaZrS_3$. The Pugh's ratio (BH/GH = 1.9) exceeds the critical value of 1.75, confirming the ductile behavior of $BaZrS_3$, which is advantageous for thin-film processing and device fabrication. The low linear compressibility coefficient (β = 0.014) implies limited compressibility, while the small universal anisotropy index (AU = 0.158) indicates weak elastic anisotropy. Overall, these results confirm that $BaZrS_3$ is mechanically stable, ductile, and suitable for practical optoelectronic and photovoltaic applications.

To study about ductile and brittle nature of substance, we use Pugh ratio which is represented by B/G ratio. If the value of pugh ratio is more than 1.75 then material is assumed to have ductile behavior. If the value of pugh ratio is smaller than 0.5, then the material is assumed to show brittle nature. As for our studying material $BaZrS_3$ the value of pugh ratio is greater than 1.75 so this material is considered to have ductile behavior.

The type of binding found in material is represented by poisson ratio **(γ).** Most of metals have poisson ratio value in range of 0.25 to 0.35. It has resemblance with 0.25 for ionic material, 0.1 for brittle covalent material and 0.33 for ductile metallic material.

We also discuss anisotropic factor for this material $BaZrS_3$which has cubic symmetry. The ratio between linear compressibility such as c and a is known as anisotropic factor. If anisotropic factor has value unity, then crystal has isotropic compressibility. It is described by following equation:

$$K_c / K_a = \frac{C11+C12-2C13}{C33-C13} \qquad 4.15$$

In this equation 4.8, along c and a axis, Kc and Ka are compressibility coefficient.

Ultimately, we discuss the universal anisotropic index A^U which is mathematically calculated as:

$$A^U = 5G_V/G_R + B_V/B_R - 6 \geq 0 \qquad 4.16$$

Material is assumed as isotropic if anisotropic index A^U has value zero. If the values for anisotropic index A^U changes from zero then material is assumed to show anisotropic nature.

Table 4.4. Optimized Structural Parameters of $BaZrS_3$

Parameter	Value
Crystal system	Cubic
Space group	Pm–3m (221)
Lattice constant (a=b=c)	5.062 Å
Unit cell volume	129.72 Å^3
Total energy	−2808.93 eV

Table 4.4 summarizes the optimized structural characteristics of $BaZrS_3$ obtained from first-principles calculations using the PBE-GGA functional. The crystal system is identified as cubic with space group Pm–3m (No. 221), confirming the formation of an ideal perovskite-type structure. The equal lattice constants along all three crystallographic axes (a = b = c = 5.062 Å) further verify the high structural symmetry of the compound.

The calculated unit cell volume of 129.72 $Å^3$ reflects a well-packed atomic arrangement, which is beneficial for structural robustness and uniform electronic behavior. The highly negative total energy value (−2808.93 eV) indicates strong interatomic bonding and confirms the thermodynamic stability of $BaZrS_3$ in its cubic phase. This stability suggests that the structure can be preserved under equilibrium conditions, making it suitable for practical material synthesis and device applications.

Overall, the optimized structural parameters demonstrate that $BaZrS_3$ is a structurally stable chalcogenide perovskite with high symmetry and favorable energetic characteristics. These results provide a reliable structural foundation for understanding the material's electronic, optical, and mechanical properties and support its potential use in photovoltaic and optoelectronic devices.

Table 4.5. Electronic Properties of $BaZrS_3$

Property	Result
Band gap type	Direct
Band gap energy	0.458 eV
High-symmetry points	Γ–X–M–Γ–R
Dominant CB states	Zr-d, Ba-s
Dominant VB states	S-p

IEER
Institute for Excellence in Education & Research

Table 4.5 summarizes the calculated electronic properties of $BaZrS_3$ obtained from density functional theory calculations using the PBE-GGA functional. The band structure analysis reveals that $BaZrS_3$ exhibits a direct band gap with a magnitude of 0.458 eV, where both the valence band maximum and conduction band minimum occur at the Γ-point. This direct nature of the band gap is highly desirable for optoelectronic and photovoltaic applications, as it enables efficient optical absorption and charge carrier transitions without the need for phonon assistance.

The electronic dispersion was evaluated along the high-symmetry path Γ–X–M–Γ–R in the Brillouin zone, ensuring a reliable representation of the electronic states throughout the reciprocal space. The orbital-resolved analysis shows that the conduction band is mainly dominated by Zr-d and Ba-s states, indicating that these orbitals play a key role in electron transport. In contrast, the valence band is primarily composed of S-p states, which contribute significantly to hole transport and bonding characteristics.

This clear separation of orbital contributions between the valence and conduction bands suggests favorable charge carrier mobility and reduced recombination losses. Overall, the electronic structure of $BaZrS_3$ highlights its strong potential as a low-band-gap semiconductor for infrared-responsive optoelectronic devices and high-efficiency photovoltaic applications.

Table 4.6. Optical Parameters at Key Energy Points

Optical Property	Peak Value	Energy (eV)
Dielectric constant (ε_2)	6.8	7.7
Absorption coefficient	Maximum	~20
Reflectivity	0.63	21
Refractive index	3.13	3.8
Energy loss function	7.5	21

Table 4.6 presents the key optical parameters of $BaZrS_3$ at characteristic energy points, highlighting its interaction with electromagnetic radiation. The imaginary part of the dielectric function (ε_2) reaches a maximum value of 6.8 at 7.7 eV, indicating strong interband electronic transitions and efficient photon absorption in this energy region. This behavior reflects a high probability of electron excitation from the valence band to the conduction band.

The absorption coefficient exhibits its maximum intensity around ~20 eV, demonstrating that $BaZrS_3$ has a strong ability to absorb high-energy photons, particularly in the ultraviolet region. The reflectivity shows a peak value of 0.63 at 21 eV, suggesting increased reflection of incident radiation at higher photon energies, which is typical for semiconducting materials with dense electronic states.

The refractive index attains a maximum value of 3.13 at 3.8 eV, signifying strong light–matter interaction and reduced light propagation speed within the material. Such a high refractive index is advantageous for optical confinement in optoelectronic devices. Additionally, the energy loss function peaks at 7.5 around 21 eV, corresponding to plasma resonance effects and collective oscillations of charge carriers. Overall, these optical characteristics confirm the suitability of $BaZrS_3$ for optoelectronic and photovoltaic applications, particularly in high-energy and ultraviolet spectral regions.

Table 4.7. Mechanical Moduli and Stability Indicators

Parameter	Value
Bulk modulus (BH)	71.37 GPa
Shear modulus (GH)	37.37 GPa
Young's modulus	Moderate
Pugh's ratio (B/G)	1.9
Poisson's ratio	0.274
Anisotropy index (AU)	0.158

Table 4.7 summarizes the mechanical moduli and stability indicators of $BaZrS_3$ derived from the Voigt–Reuss–Hill approximation. The calculated bulk modulus (BH = 71.37 GPa) indicates a moderate resistance to volume change under applied pressure, reflecting the material's structural robustness. Similarly, the shear modulus (GH = 37.37 GPa) suggests adequate resistance to shear deformation, which is essential for maintaining mechanical integrity under external stress.

The Young's modulus is described as moderate, implying that $BaZrS_3$ exhibits balanced stiffness, neither excessively rigid nor overly flexible. This characteristic is favorable for thin-film deposition and mechanical processing. The Pugh's ratio (B/G = 1.9) exceeds the critical threshold of 1.75, clearly indicating the ductile nature of the material. Ductility is an important property for practical device fabrication, as it reduces the risk of mechanical failure during handling and operation. The calculated Poisson's ratio (0.274) falls within the typical range for ductile and partially ionic solids, suggesting a mixed bonding character in $BaZrS_3$. Furthermore, the low universal anisotropy index (AU = 0.158) indicates weak elastic anisotropy, meaning the mechanical properties are nearly isotropic. Overall, these results confirm that $BaZrS_3$ is mechanically stable, ductile, and suitable for optoelectronic and photovoltaic device applications.

Conclusion

With the use of CASTEP program by applying generalized gradient approximation (PBE-GGA) approach inside density functional theory (DFT) the first principle simulation of structural, optical, electronic and mechanical characteristics of material $BaZrS_3$ has been performed. Cubic structure of the material $BaZrS_3$ has been found in space group and number Pm -3m, 221 respectively and the unit cell volume is found $129.72(A^o)^3$. The lattice parameters of material $BaZrS_3$ are $a=b=c=5.062A^o$. The total energy of the studying material is -2808.93eV. The structural properties indicate that $BaZrS_3$ has the stable structure. The electronic energy gap for the material $BaZrS_3$ have been calculated which is found to be 0.458eV. The band gap of compound $BaZrS_3$ describes that maxima of valance band and minima of conduction band are located at same K- point G which implies that $BaZrS_3$ has direct band gap. The partial density of states has been found by using CASTEP method. The optical properties such as energy loss function, refractive index, conductivity, dielectric function, reflection and absorption coefficient of $BaZrS_3$ have been found in energy range of 0–60eV. These optical characteristics demonstrate that material $BaZrS_3$ is suitable for solar applications and optoelectronic devices. The mechanical properties of material $BaZrS_3$ have also been calculated which shows that all the elastic constant have positive values and describes that structure is mechanically stable. The mechanical characteristics are studied by implementing Voigt-Reuss-Hill approximation and have been checked by stress-strain approach to know that structure is mechanically stable. The universal anisotropic coefficient of the material have been calculated which indicate that material have anisotropic behavior. The calculated value of pugh ratio (B/G) describes that material have ductile nature as its value is greater than 1.75. Its composition proves it useful to be used in semiconductor devices. The results from the study of material $BaZrS_3$ leads to groundwork for future use in photovoltaic devices.

Despite providing a comprehensive first-principles analysis of the structural, electronic, optical, and mechanical properties of $BaZrS_3$, this study has certain limitations. The calculations were performed using the PBE-GGA functional, which is known to underestimate band gap values; therefore, the reported electronic gap may deviate from experimental results. Advanced approaches such as hybrid functionals (HSE06) or many-body perturbation methods (GW) could yield more accurate electronic and optical predictions. Additionally, the present work is restricted to zero-temperature and zero-pressure conditions, whereas real device operation involves thermal effects, strain, and environmental exposure. Phonon dispersion and finite-temperature stability were not explored, which limits insights into lattice

dynamics and thermal transport behavior. Moreover, defect states, surface effects, and grain boundaries—critical factors influencing carrier recombination and device efficiency—were not considered.

Future work should focus on incorporating temperature-dependent properties through ab initio molecular dynamics and phonon calculations to assess thermal stability and vibrational characteristics. The influence of intrinsic defects, dopants, and strain engineering on electronic and optical performance should also be systematically investigated. Experimental validation of the predicted properties, along with device-level simulations for photovoltaic and optoelectronic applications, would further strengthen the applicability of $BaZrS_3$. Such studies will help bridge the gap between theoretical predictions and practical implementation in renewable energy technologies.

References

Gielen D, Boshell F, Saygin D, Bazilian MD, Wagner N, Gorini R (2019) The role of renewable energy in the global energy transformation. Energy Strateg Rev 24(January):38–50

U.S. Energy Information Administration (2050) International energy outlook 2019 with projections to 2019

https://blog.bccresearch.com/a-history-of-perovskite-solar-cells

NREL. https://www.nrel.gov/pv/cell-efciency.html

Bin H, Gao L, Zhang ZG, Yang Y, Zhang Y, Zhang C, Chen S, Xue L, Yang C, Xiao M, Li Y (2016) 11.4% efciency non-fullerene polymer solar cells with tri-alkylsilyl substituted 2D-conjugated polymer as donor. Nat Commun 7:13651

Gnes S, Neugebauer H, Sariciftci NS (2007) Conjugated polymer-based organic solar cells. Chem Rev 107(4):1324–1338

Grossiord N, Kroon JM, Andriessen R, Blom PWM (2012) Degradation mechanisms in organic photovoltaic devices. Org Electron 13(3):432–456

Sanehira EM, Marshall AR, Christians JA, Harvey SP, Ciesielski PN, Wheeler LM, Schulz P, Lin LY, Beard MC, Luther JM (2017) Enhanced mobility CsPbI3 quantum dot arrays for record-efciency, high-voltage photo-voltaic cells. Sci Adv 3(10):eaao4204

Gratzel M (2001) Photo electrochemical cells. Nature 414(6861):338–344

Dette C, Prez-Osorio MA, Kley CS, Punke P, Patrick CE, Jacobson P, Giustino F, Jung SJ, Kern K (2014) TiO2 anatase with a bandgap in the visible region. Nano Lett 14(11):6533–6538

Mitzi DB, Wang S, Feild CA, Chess CA, Guloy AM (1995) Conducting layered organic–inorganic halides con-taining oriented perovskite sheets. Science 267(1473):35

Mitzi DB, Chondroudis K, Kagan CR (2001) Organic-inorganic electronics. IBM J Res Dev 45(29):36

Topsöe H (1884) Krystallographisch-chemische untersu-chungen homologer verbindungen. Z Krist 8:246

https://en.m.wikipedia.org/wiki/Chalcogen

https://www.sigmaaldrich.com/PK/en/products/materials-science/energy-materials/chalcogenides

Franzen, H.F.; Beineke, T.A.; Conrad, B.R. (1968). "The crystal structure of Nb21S8". Acta crystallographic B. 24 (3): 412–p416.https://doi.org/10.1107%2FS0567740868002463

Y.-Y. Sun, M.L. Agiorgousis, P. Zhang, S. Zhang, Chalcogenide perovskites for photovoltaics. Nano Lett. 15, 581–585 (2015)

A.H.S. Reshak, S. Khan, A. Laref, G. Murtaza, J. Bila, Pressure induced physical variations in the lead free fluoropervoskites XYF3 (X - K, Rb, Ag;Y - Zn, Sr, Mg): optical materials. Opt. Mater. 109, 110325 (2020).https://doi.org/10.1016/j.optmat.2020.110325

https://doi.org/10.1007/s11051-022-05525-0

Arif Khalil, R.M., Hussain, M. I., Saeed, N., Rana, A. M., and Hussain, F. (2021). The prediction of structural, electronic, optical and vibrational behavior of ThS_2 for nuclear fuel application: A DFT Study. *Optical and quantum electronics, 53, 1–15.*

Azzouz, L., Halit, M., H., Denawi and Matta, C.F. (2020). Magnetic semiconductor properties of $RbLnSe_2$ (Ln= Ce, Pr, Nd, Gd); a DFT Study. *Journal of magnetism and magnetic materials, 501, 166448.*

Bounchenafa, M., Benmakhlouf, A., S., ..., and Al-Douri, Y. (2020). Theoretical investigation of structural, elastic, electronic and optical properties of ternary tetragonal tellurides KBTe2 (b=Al, Ln). *Material science in semiconductor processing, 114, 105085.*

IEER
Institute for Excellence in Education & Research